Journal of Applied Polymer Science

Bio-nanocomposite films based on cellulose nanocrystals filled polyvinyl alcohol/chitosan polymer blend

Nassima El Miri,[1,2] Karima Abdelouahdi,[3] Mohamed Zahouily,[1] Aziz Fihri,[2] Abdellatif Barakat,[4] Abderrahim Solhy,[5] Mounir El Achaby[5]

[1]Faculté des Sciences et Techniques, Université Hassan II-Casablanca, Casablanca 20650, Morocco
[2]MAScIR Foundation, Rabat Design, Rue Mohamed El Jazouli, Madinat Al Irfane 10100 Rabat, Morocco
[3]Division UATRS, Centre National pour la Recherche Scientifique et Technique (CNRST), Angle Allal Fassi/FAR, Hay Riad, 10000 Rabat, Morocco
[4]INRA, UMR 1208 Ingénierie des Agropolymères et Technologies Emergentes (IATE) 2, 34060 Montpellier Cedex 1, France
[5]Université Mohammed VI Polytechnique, Lot 660-Hay Moulay Rachid, 43150 Ben Guerir, Morocco
Correspondence to: A. Solhy (E-mail: abderrahim.solhy@um6p.ma) and M. El Achaby (E-mail: mounir.elachaby@um6p.ma)

ABSTRACT: Bio-nanocomposite films based on polyvinyl alcohol/chitosan (PVA/CS) polymeric blend and cellulose nanocrystals (CNC) were prepared by casting a homogenous and stable aqueous mixture of the three components. CNC used as nanoreinforcing agents were extracted at the nanometric scale from sugarcane bagasse via sulfuric acid hydrolysis; then they were characterized and successfully dispersed into a PVA/CS (50/50, w/w) blend to produce PVA/CS–CNC bio-nanocomposite films at different CNC contents (0.5, 2.5, 5 wt %). Viscosity measurement of the film-forming solutions and structural and morphological characterizations of the solid films showed that the CNC are well dispersed into PVA/CS blend forming strong interfacial interactions that provide an enhanced load transfer between polymer chains and CNC, thus improving their properties. The obtained bio-nanocomposite films are mechanically strong and exhibit improved thermal properties. The addition of 5 wt % CNC within a PVA/CS blend increased the Young's modulus by 105%, the tensile strength by 77%, and the toughness by 68%. Herein, the utilization of Moroccan sugarcane bagasse as raw material to produce high quality CNC has been explored. Additionally, the ability of the as-isolated CNC to reinforce polymer blends was studied, resulting in the production of the aforementioned bio-nanocomposite films with improved properties.
 J. Appl. Polym. Sci. **2015**, *132*, 42004.

KEYWORDS: biopolymers and renewable polymers; blends; composites; mechanical properties; properties and characterization

Received 24 September 2014; accepted 17 January 2015
DOI: 10.1002/app.42004

INTRODUCTION

Recently, more attention has been given to natural polymers with a focus on sustainable development and environmental preservation.[1] Following this tendency, the attempt has been made to replace polymers derived from petroleum with superior biodegradable polymers.[2] In this context, biopolymers are considered potential replacements for conventional plastic materials; nevertheless, some of their properties must be improved to position them as materials that can be competitive with fossil derivatives, especially their poor mechanical, thermal, and barrier properties.[3] The use of natural polymers has several advantages including non-toxicity, biodegradability, wide availability, and biocompatibility, especially when compared to their synthetic counterparts.[2]

Chitosan (CS) is a linear polysaccharide and deacetylated derivative of chitin.[4] This biopolymer is among the most important natural polymers due to its diverse spectrum of applications that range from pharmaceuticals to materials science.[5–8] However, some obstacles hinder CS's extensive use, particularly, its relatively lower elongation, low toughness properties, high degree of swelling in water, relatively poor water vapor barrier characteristics as well as its high price compared to conventional plastics.[9,10] In an effort to overcome these scientific and technological challenges, several attempts have been made to improve the properties of CS, particularly for the CS-based film. For example, to improve the mechanical and functional properties of CS film, several synthetic polymers have been blended with CS such as poly(vinyl

Additional Supporting Information may be found in the online version of this article.

pyrrolidone), poly(vinyl alcohol), poly(ethylene oxide), polycaprolactone, and polyacrylamide.[6,11]

Polyvinyl alcohol (PVA) is a material with technological potential as a water-processable polymer. It has a wide commercial application due to its unique chemical and physical properties.[12–14] PVA is a nontoxic, highly crystalline, and a water-soluble polymer that has good film-forming ability and high hydrophilic properties, which arise from the presence of —OH groups and the hydrogen bond formation. PVA has been widely used for the preparation of blends and composites with several natural polymers, such as chitosan, alginate, carboxymethyl cellulose, and starch.[12,15–19]

Polymer blending is one of the most effective methods to create new materials with desired properties.[11] Films produced from the blending of polymers usually exhibit modified properties as compared to films made from an individual component.[11] As synthetic polymers are easily obtained and have a relatively low production cost, blending of natural and synthetic polymers may improve the cost performance ratio of the resulting films.[16,17,20,21] CS contain hydroxyl and amine groups and are potentially miscible with PVA due to the formation of hydrogen bonds.[15,19,21] Indeed, the combination of these properties allows the formation of a PVA/CS blend that may lead to the preparation of new biocompatible and a homogeneous blend matrix for bio-nanocomposite development.

Conversely, nanocomposite technology using nanofillers has already been proven as an effective way to produce new materials with specific properties and high performances.[22,23] The nanocomposites consist of a polymeric matrix (continuous phase) and a filler (discontinuous phase), where at least one dimension is $<$100 nm. The nanometric dimension and the type of the nanofiller provide a synergic effect to the material, improving the resulting properties of the nanocomposites when compared with those of the host matrix.[22,23] Nanoreinforcements are unique in that they do not affect the clarity of the polymer matrix. They appear transparent as they are smaller than the wavelength of visual light.[24] Only a few percentages of these nanomaterials are normally incorporated (0.5–5%) into the polymer and the improvement is vast due to their high surface area.[25]

With the emergence of nanostructured polymer nanocomposites, incorporating elongated cellulose nanocrystals (CNC) has attracted more and more attention in the field of nanotechnology.[26–28] CNC, which can be sphere-like, rod-like, ribbon-like, or needle-like shape, have a length ranging from 100 nm up to 1–2 μm, and a diameter of about 5–20 nm.[29] The main features that stimulate the use of CNC as polymer reinforcement agents are its large specific surface area (estimated to be several hundreds of $m^2\ g^{-1}$) and its very high modulus of elasticity (approximately 150 GPa).[28,30] Other attractive advantages of CNC are its low density (about 1.566 g cm^{-3}), biocompatibility, and biodegradability. Additionally, CNC can be extracted from abundant and renewable natural sources.[31] Among these sources, sugarcane bagasse (SCB) is widely used as bio-sourced materials to obtain CNC.[32–35] SCB is annually produced in large quantities throughout the world, in areas such as Brazil,[36,37] India,[38] Cuba,[36] China,[36] México,[37] Indonesia,[39] Colombia,[40] and Morocco. Currently in Morocco, about 90% of this residue is used for combustion in energy production. Climate and the weather conditions have a great potential to alter the shape and structure of SCB and biomass in general. Taking into consideration these major global ecological concerns, the proposed method of this study provides a new approach to valorize the Moroccan SCB by designing and preparing biopolymer-blend based bio-nanocomposite films with an expected outcome of use in cutting-edge industries.

The aim of this study was to explore the utilization of Moroccan SCB as a source of raw material for the production of CNC using sulfuric acid hydrolysis. Several techniques were used to characterize the materials at different stages of treatment, starting from raw SCB to the isolation of CNC. Then, the obtained CNC was dispersed into a PVA/CS polymer blend to fabricate PVA/CS–CNC bio-nanocomposite films via the solution casting technique, where CNC acted as the cross-linker because of its multifunctional groups on its surfaces, especially hydroxyl and sulfate groups. Herein, this functionality of CNC ensures their compatibility with the PVA/CS biopolymer blend. Because these polymers have also the large number of functional groups, including hydroxyl groups of PVA and hydroxyl and amino groups of CS. This compatibility between the CNC and the blend can cause noncovalent interactions, therefore driving the formation of a complex network in PVA/CS–CNC system. Rheological measurement of film-forming solutions and the structural, thermal, and mechanical properties of the as-prepared bio-nanocomposite films were evaluated and further discussed in this report.

EXPERIMENTAL

Materials

The sugarcane bagasse (SCB) was provided by a SUNABEL-COSUMAR Group, a company located in the region of Gharb-Loukkos, Morocco. First, the SCB was ground using a precision grinder (Fritsch-Pulverisette 19, GmbH) equipped with a 1 mm sieve. Then, this fraction was sifted in a 150 μm size sieve (Fritsch mesh) to remove the small particles. The moisture content of the bagasse was about 7%. Polyvinyl alcohol (molecular weight: 10,000–26,000; 86–89% hydrolyzed) and chitosan (molecular weight: 110,000–150,000; degree of acetylation $\leq$40 mol %) were purchased from Alfa-Easer and Aldrich, respectively. Analytical grade chemicals used for extraction, bleaching, and hydrolysis were purchased from Sigma–Aldrich and used without further purification.

Isolation and Physical Aspect of CNC

CNC used as nanoreinforcing agents have been extracted from SCB throughout the three well know steps, alkali treatment, bleaching, and acid hydrolysis (Figure 1). The detail of these steps is given in Supporting Information. Visually, the initial ground SCB had a yellow-brown color (Figure 1), with fibrous structure and each fiber appeared to be composed of several fibrils. These fibrils were associated in small bundles and cemented by non-cellulosic compounds, showing a complete and compact structure along each elementary SCB fiber, and exhibiting an alignment in the fiber axis direction as shown by SEM analysis (Supporting Information Figure S1). Beginning

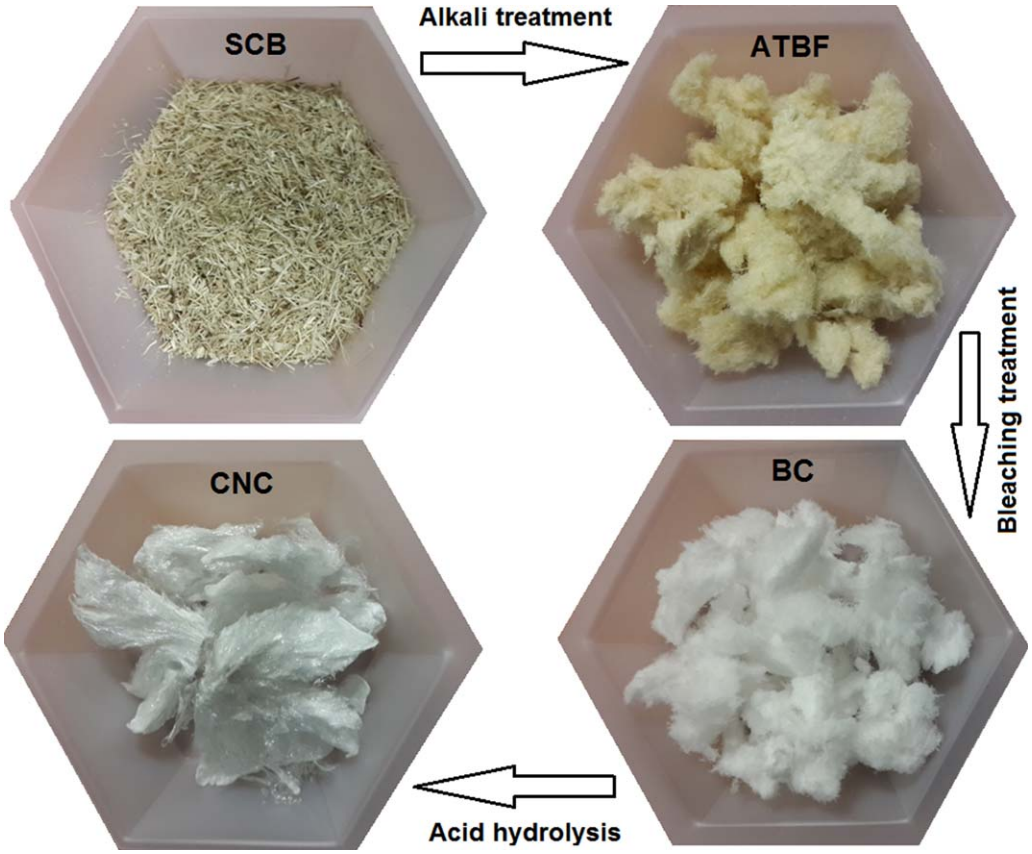

Figure 1. Physical aspect of SCB, ATBF, BC, and CNC samples. [Color figure can be viewed in the online issue, which is available at wileyonlinelibrary.com.]

with the alkali treatment of the raw SCB fibers, the main focus of this step was to partially eliminate the whole non-cellulosic components (lignin, hemicelluloses, and pectin), resulting in the alkali-treated bagasse fibers (ATBF).[41] With the subsequent treatment of alkali, some alkali-labile linkages (ether and ester linkages) between lignin monomers or between lignin and polysaccharides may have been broken, which helped in the partial defibrillation of fibers. This treatment yielded about 45% yellow colored fibers (Figure 1), which was calculated by the weight of the obtained fibers divided by the initial weight of SCB. The next step was the bleaching treatment with the aim to purify the cellulosic fibers from any residual lignin or others impurities obtained after the alkaline treatment. This bleaching treatment can result in the total defibrillation of fibers into individual microfibrils with smaller diameter. The bleached cellulose fibers (BC) might have contained pure cellulose, shown by a clearly white color (Figure 1), thus confirming that the residual non-cellulosic elements were totally removed under the bleaching treatment, as confirmed by FTIR measurements (Supporting Information Figure S2). The yield of this bleached product was about 33% in regard to the initial amount of SCB. The third and final step was the performance of acid hydrolysis, which was performed under appropriate conditions that allowed the removal of amorphous domains from the bleached cellulose. The removal of amorphous domains, via acid hydrolysis, was performed by cleaving cellulose microfibrils into bundles of CNC with nanometric dimensions, becoming more or less individualized by sonication with the ability to be obtained in a clearly white powdered form via a freeze-drying process (Figure 1). The yield of CNC was 15% with respect to the initial amount of dried SCB fibers, and 45% with respect to the amount of bleached cellulose.

Films Preparation

The PVA/CS–CNC films were prepared by the casting/evaporation technique. First, 1.5 g of PVA was dissolved in 40 mL of water, under continuous stirring, for 1 h at 90°C; at the same time, 1.5 g of CS was dissolved in 100 mL of 1% aqueous acid acetic solution at 50°C, with constant stirring for 1 h. The obtained PVA and CS solutions were cooled until ambient temperature was reached. Then, the two solutions were mixed together under mechanical stirring for 1 h at 25°C, resulting in a homogeneous solution of PVA/CS (50/50; w/w ratio). The desired amount of CNC (0.5, 2.5, and 5 wt % in regard to PVA/CS mass) was dispersed in 20 mL of water and sonicated for 30 min in an ice bath to obtain a homogenous suspension. The CNC were gradually added to the PVA/CS mixture under vigorous stirring for 30 min. The obtained PVA/CS–CNC mixture was sonicated for another 30 min to achieve dispersion of the CNC in the blend. Subsequently, the PVA/CS–CNC mixture was casted onto a plastic disk and the water evaporated at an ambient temperature. Finally, the obtained films were dried for 4 h at 60°C and for 1 h at 80°C. PVA/CS blend, neat PVA, and neat CS films were also prepared according to the same process mentioned above, without the addition of the CNC. The films were coded PVA,

CS, PVA/CS, PVA/CS-0.5, PVA/CS-2.5, and PVA/CS-5. The number in the three last code names indicates the weight fraction of CNC in regard to PVA/CS mass.

Characterization Techniques

Atomic force microscopy (AFM) measurement was performed using a Veeco Dimension ICON. Tapping mode was used to capture height and phase images at a scan rate of 1.5 Hz. The samples used for AFM characterizations were deposited from CNC dispersion on mica sheets. The zeta potential measurement of CNC dispersion was performed using a Malvern Zetasizer Nano ZS instrument. The surface charge density of CNC was calculated by conductometric titration method reported by Jiang *et al.*[42] briefly, 50 g portions of 0.5 wt % CNC suspension, containing 1 m*M* sodium chloride, were titrated under nitrogen with a 0.02*N* sodium hydroxide solution. Both pH and conductivity were recorded by a pH electrode (Inlab 413, Mettler-Toledo International) and conductivity electrode (EC300, VWR International). From the volume of NaOH used to titrate the sulfate groups, the charge density of CNC could be determined: mmol of RSO_3^-/kg CNC = $(C_{NaOH} \times V_{NaOH})/m_{CNC}$. Where C_{NaOH} is the concentration of the titrant NaOH, V_{NaOH} is the volume at the equivalence point, and m_{CNC} is the mass of CNC used for the measurement. X-ray diffraction (XRD) characterizations were performed using a Bruker D8 Discover using the Cu Kα radiation ($\lambda = 1.54184$ nm) in the 2θ range of 2–60° while the voltage and current were held at 45 kV and 100 mA. The steady shear viscosity measurement of film-forming solutions was performed at 20°C, using a rotational Physica MCR500 rheometer equipped with concentric cylinder geometry (CC27). The temperature was regulated by a Paar Physica circulating bath and a controlled peltier system (TEZ 150P-C). Transform infrared spectroscopy (FTIR) was performed on an ABB Bomem FTLA 2000 spectrometer equipped with a Golden Gate single reflection ATR accessory. Morphology of films was evaluated at their fracture surface, using a scanning electron microscope (SEM) (FEI, Quanta 200-ESEM) operating at 20 kV. Samples were cryofractured before being coated by a thin conductive carbon layer to help improve SEM observations. Thermogravimetric analyses (TGA) were conducted with a 10°C min^{-1} heating rate from 25 to 700°C, using a TGA-Q500 (TA Instrument). Differential scanning calorimetry (DSC) was performed under nitrogen gas with a 10°C min^{-1} heating rate from −50°C to 270°C, using a DSC-Q100 (TA Instrument) and the sample mass was approximately 10 mg for each sample. Tensile tests were performed using an Instron 8821S tensiometer. The tensile specimens were cut in rectangular shapes with dimensions of 80 mm in length and 10 mm in width. The gauge length was fixed at 30 mm and the speed of the moving clamp was 5 mm·min^{-1}. All tests were performed on a minimum of five samples and the reported results are average values.

RESULTS AND DISCUSSION

Characterization of CNC

The stability of the CNC suspension is crucial in the preparation of nanocomposites and can be derived from the zeta potential of the CNC suspension and the surface charge density of CNC. It is well-known that the stability of CNC depends strongly on its aspect ratio, surface functionalization, and the

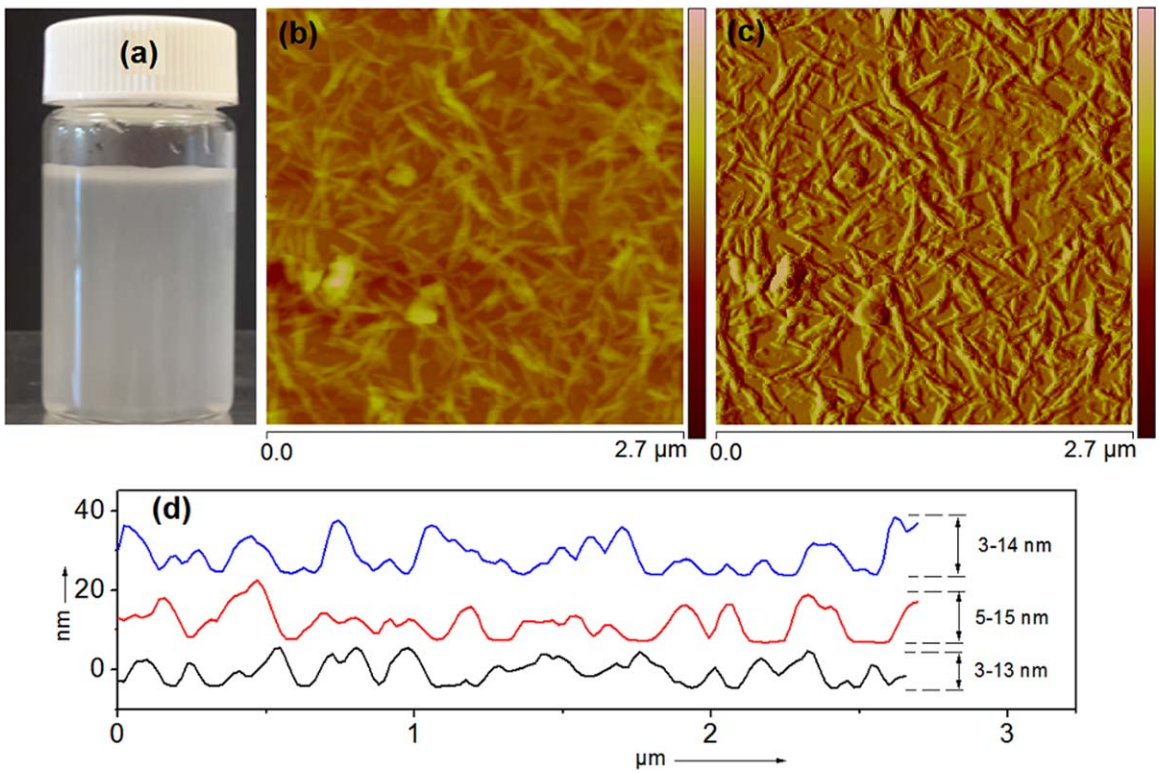

Figure 2. (a) Aqueous suspension of CNC (6.8 mg mL^{-1}) and (b) height and (c) amplitude tapping mode AFM images of CNC; (d) represent the height profiles taken along the image at three different positions. [Color figure can be viewed in the online issue, which is available at wileyonlinelibrary.com.]

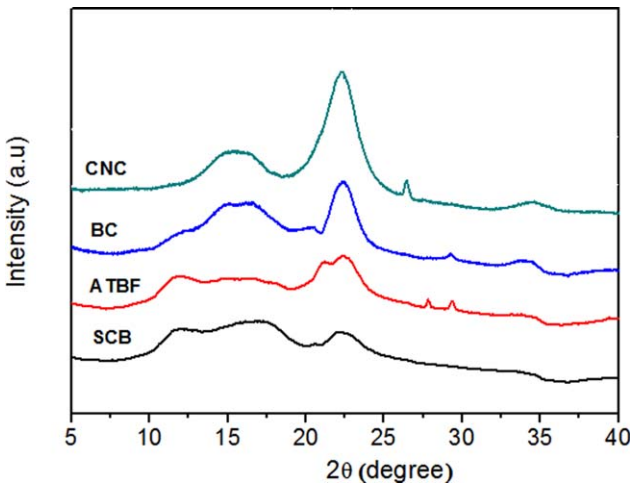

Figure 3. XRD patterns of SCB, ATBF, BC, and CNC samples. [Color figure can be viewed in the online issue, which is available at wileyonlinelibrary.com.]

ability of the solvent and surface groups to counterbalance the attractive hydrogen-bond interactions exerted by the abundant hydroxyl groups.[43] Figure 2(a) shows photograph illustrating the CNC aqueous suspension stability, in which a white gel appearance is observed for the as-isolated CNC dispersion. Some reasons for good stability of CNC dispersion is the exclusion of apolar components, the insertion of polar sulfate groups, and the exposition of —OH groups from the cellulose structure. For our CNC suspension, the zeta potential had a mean value of −54.3 mV (Supporting Information Figure S3). The suspension of CNC was considered stable because the absolute value was higher than 25 mV.[44,45] Additionally, the surface charge density of the CNC was determined by conductometric titration with sodium hydroxide,[42] and the obtained average value was 162 mmol kg^{-1}, confirming the attachment of anionic sulfate groups onto the surface of the CNC after acid treatment.[46]

The morphology and size of the as-obtained CNC were characterized by AFM analysis; the micrographs are shown in Figure 2(b,c). It has been reported that AFM is a better method to characterize the CNC, because it provides some informations about the diameter, length, and shape of the CNC.[43,46] AFM images show that the as-isolated CNC had needle-like nanoparticles, thus confirming that their extraction from the treated SCB was successful. These images show individual CNC and some aggregates through transverse height profiles. The appearance of laterally aggregated elementary crystallites in AFM images is expected due to the high specific area and strong interaction bonds established between the CNC. Additionally, AFM images show that CNC are uniform in diameter and irregular in length. In general, the exact dimensions of the CNC depend on the nature of the original raw material and hydrolysis conditions or pretreatments.[47] Herein, the dimensions of CNC were approximately calculated by the high profiles taken along the CNC high sensor image [Figure 2(d)]. It is clear that the diameter of the extracted CNC was found to be in nanometric scale, ranging from 3 to 15 nm with the length ranging from 100 to 300 nm. These results are in strong agreement with the observations of Teixeira *et al.*,[33] especially in relation to the geometry and diameter scale for the CNC obtained from SCB by 6*M* sulfuric acid hydrolysis and also for CNC obtained from others lignocellulosic materials.[48,49]

To study the crystalline structure and the crystallinity index (CrI) of SCB, ATBF, BC, and the as-isolated CNC, the XRD analysis was performed and the obtained results are shown in Figure 3. For all samples, the major intensity peaks are located at $2\theta = 14.9°$, 16.3°, 22.4°, and 34.5°, which correspond to the (1 0 1), (1 0 $\bar{1}$), (0 0 2), and (0 0 4) planes.[46,50] These results indicate that there is a predominance of crystalline structure of cellulose I for all cellulosic samples. Though the XRD data of SCB, ATBF and BC display a small amount of cellulose II polymorph, which can be verified by the presence of small peak observed at $2\theta \approx 11.7°$ and 20.5°.[46,50] Contrary, the hydrolyzed CNC exhibit only a crystalline structure of cellulose I. From the XRD data, the crystallinity index (CrI) was determined using the procedure previously described,[46,50] using $CrI = [(I_{002} - I_{amorph})/I_{002}] \times 100$ equation. Herein, we consider that the I_{002} is the principal intensity of the crystalline portion of cellulose at $2\theta = 22.4°$, and the I_{amorph} is the intensity of the amorphous portion of cellulose and other

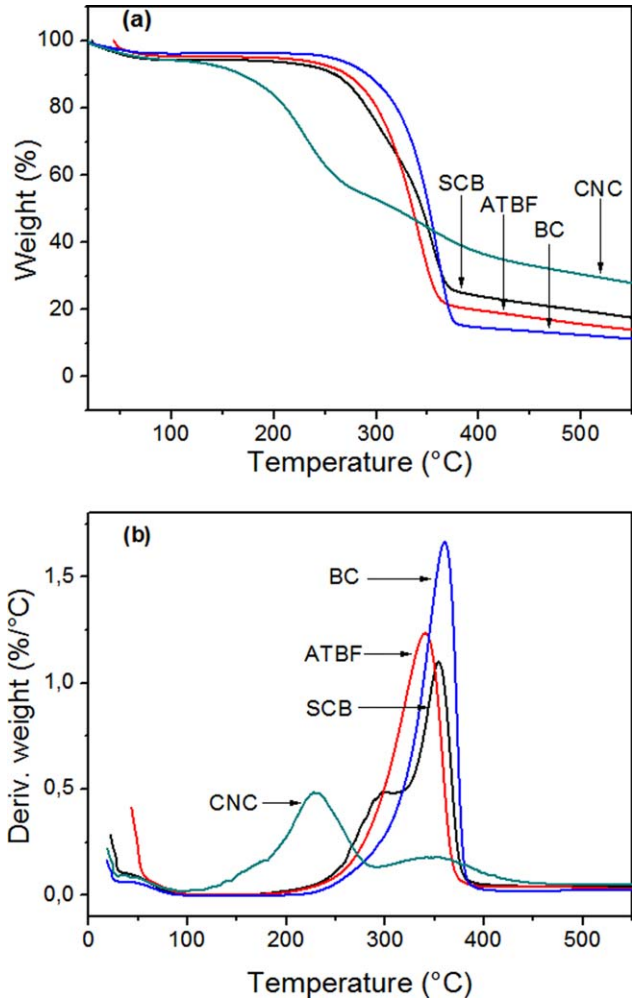

Figure 4. (a) ATG and (b) DTG curves of SCB, ATBF, BC, and CNC samples. [Color figure can be viewed in the online issue, which is available at wileyonlinelibrary.com.]

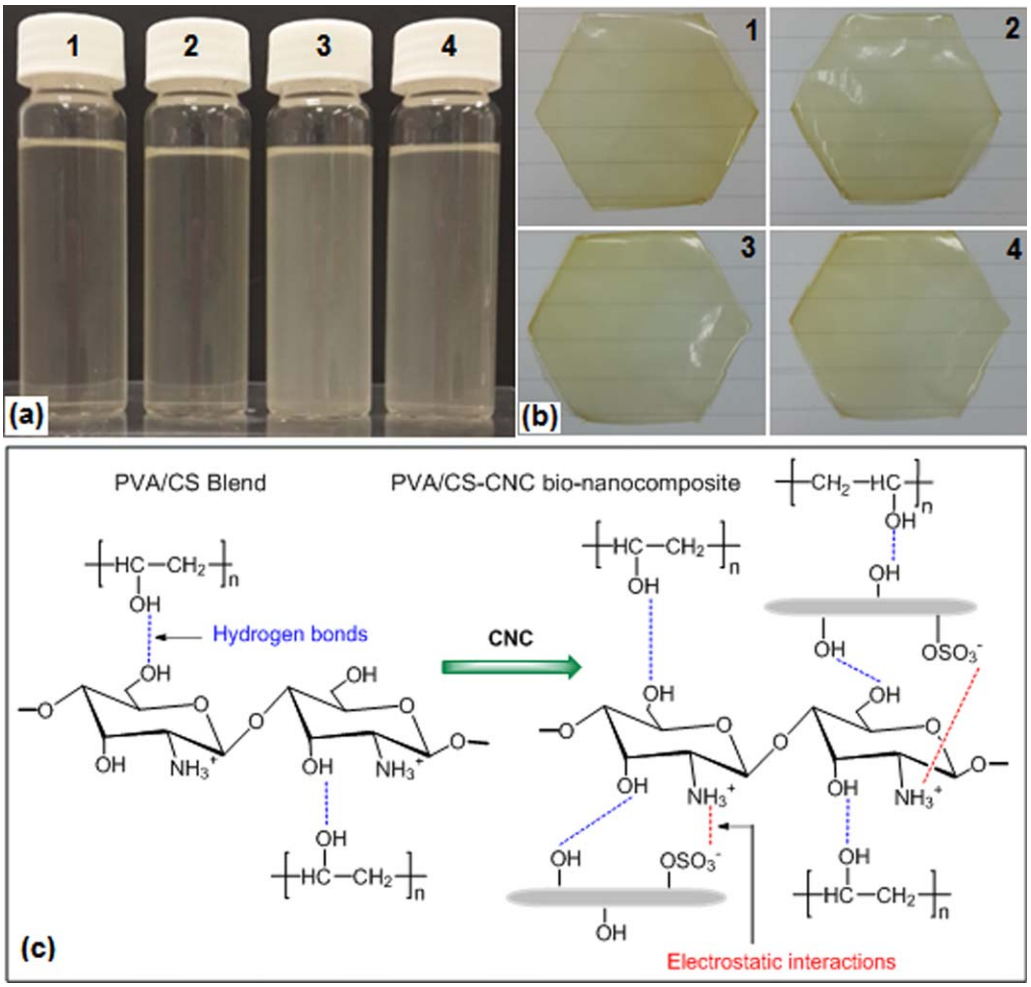

Figure 5. Digital images of (a) film-forming solutions and (b) the corresponding isolated solid films with (1) PVA/CS, (2) PVA/CS-0.5, (3) PVA/CS-2.5, and (4) PVA/CS-5 and (c) the schematic of intermolecular hydrogen bonds and electrostatic interactions that occurred in PVA/CS and PVA/CS–CNC bio-nanocomposite films. [Color figure can be viewed in the online issue, which is available at wileyonlinelibrary.com.]

constituents, which is reported to occur at around $2\theta \approx 18.5°$ in the literature.[51] By this method, the CrI was found to be about 19%, 36%, 45%, and 77% for the SCB, ATBF, BC, and CNC samples, respectively. The increasing of CrI from SCB to CNC was ascribed to the progressive removal of amorphous non-cellulosic materials, as confirmed by FTIR analysis of materials at different stages of treatment (Supporting Information Figure S2). The subsequent increase of the CrI value upon acid hydrolysis of purified cellulose (BC) fibers is indicative of the dissolution of amorphous cellulosic domains.

To investigate the thermal degradation of all cellulosic samples (SCB, ATBF, BC, and CNC), a thermogravimetric analysis was performed, and the TGA and DTG curves obtained in nitrogen atmosphere are illustrated in Figure 4(a,b). The onset temperatures, T_{onset} (corresponding to a weight loss of 8%) of raw SCB, ATBF, and BC fibers were observed at 239, 257, and 279°C, respectively [Figure 4(a)]; and the corresponding maximum temperatures (T_m) were observed at 355, 341, and 359°C, respectively [Figure 4(b)]. For CNC, the T_{onset} is reduced to 150°C and the T_m is reduced to 230°C. These lower T_{onset} and T_m observed for CNC, as compared to those of SCB, ATBF, and BC, is due to the insertion of sulfate groups in the surface of CNC during hydrolysis with sulfuric acid.[33,43,45]

Processing of Films

The mixture of PVA/CS, and CNC in water can be easily achieved in controlled conditions, enabling the formation of a homogeneous and stable aqueous mixture. Figure 5(a) shows the photographs of a PVA/CS solution and its PVA/CS–CNC mixtures with different amounts of CNC (0.5, 2.5, and 5 wt %). The photographs were recorded at room temperature 15 days after the preparation of the mixtures, showing high stability and good homogeneity. By casting these solutions on plastic dishes and evaporating of solvent, films with high quality, smooth surface, good flexibility, and 50-μm-thick were produced. Figure 5(b) shows the isolated films of unloaded PVA/CS and its PVA/CS–CNC bio-nanocomposites with different amounts of CNC. As shown in the images, the visual transparency of PVA/CS was not affected by the addition of different amounts of CNC, indicating that the three components were well mixed in the chosen conditions of preparation. We noted that the thickness of these films could be controlled by the amount of the solution used

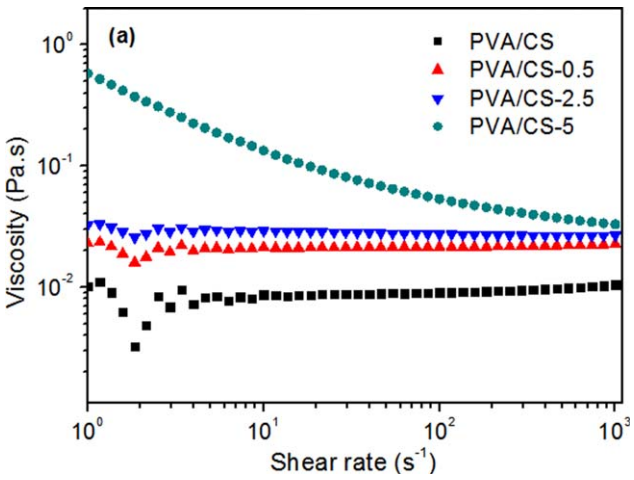

Figure 6. Viscosity curves of film-forming solutions of PVA/CS, PVA/CS-0.5, PVA/CS-2.5, and PVA/CS-5 bio-nanocomposites. [Color figure can be viewed in the online issue, which is available at wileyonlinelibrary.com.]

for the casting technique. Furthermore, it could simply be cut into various desired forms by a special knife.

It is well known that PVA and CS are miscible polymers via hydrogen bonding interactions [Figure 5(c)] because both polymers contain free hydroxyl groups.[15,19,21] Also, their mixture in water is easily achieved due to their hydrophilic nature. Interestingly, the sulfuric acid hydrolyzed CNC exhibits free hydroxyl and inserted anionic sulfate groups on their surfaces, which can also strongly interact with free hydroxyl groups of PVA,[52] and free hydroxyl and amine groups of CS.[53,54] In this way, when CNC are added to the PVA/CS mixture, an interconnected bond network can be formed throughout strong electrostatic interactions and hydrogen bonding, as proposed in Figure 5(c). This behavior can be deduced from the viscosity measurement of film-forming solutions and FTIR analysis (see below).

Viscosity of Film-Forming Solutions

Figure 6 exhibits the dependence of the steady shear viscosity (η) on the shear rate ($\dot{\gamma}$) for film-forming solutions of the PVA/CS mixture blend and its PVA/CS–CNC bio-nanocomposite mixtures obtained from the steady shear sweep. It should be noted that all solutions were prepared under the same conditions (solvent volume, temperature, time, and stirring). The PVA/CS blend showed a Newtonian behavior in the full shear rate range, which was characterized by the shear rate-independent viscosity. Furthermore, PVA/CS-0.5 and PVA/CS-2.5 bio-nanocomposite mixtures exhibited the same behavior as unloaded PVA/CS (Newtonian behavior), with increases in shear viscosity for the entire shear rate range (Figure 6). When 5 wt % CNC was added, the PVA/CS-5 showed only shear thinning behavior characterized by the decrease of the viscosity with the increase of the shear rate. This change in the viscosity was due to the flow-impeding effect induced by the presence of CNC, which limited the shear flow of the macromolecule chains of polymers, and resulted in an increase of shear viscosity of PVA/CS–CNC film-forming solutions. Moreover, due to the high affinity between the functional groups of PVA, CS, and CNC, the CNC formed a bond network throughout strong electrostatic interactions and hydrogen bonding between CNC and polymer blend chains [Figure 5(c)], restricting the mobility of macromolecule chains of polymers.

FTIR Characterization of Films

The FTIR measurements were performed to investigate the structure of PVA/CS and PVA/CS–CNC bio-nanocomposite films. Figure 7 shows the FTIR spectra of CNC and PVA/CS based films, while the spectra of neat PVA and CS films are presented in Supporting Information Figure S4.

From Supporting Information Figure S4, for the CS spectrum, the band at 3348 cm^{-1} is associated to O—H and N—H hydrogen band stretches. The bands at 2975 and 2906 cm^{-1} are attributed to C—H stretching. The band at 1687 cm^{-1} is due to C—O stretching of the acetyl group. The band at 1592 cm^{-1} is associated to N—H bending and stretching. The bands at 1462 cm^{-1} are associated to asymmetrical C—H bending of CH_2 group.[55] For pure PVA (Supporting Information Figure S4), the band at approximately 3358 cm^{-1} is assigned to —OH stretching, and that at 1478 cm^{-1} corresponds to OH bending vibration of hydroxyl group. The band corresponding to methylene group (CH_2) asymmetric stretching vibration occurs at about 2987 cm^{-1}. The vibrational band at about 1743–1586 cm^{-1} corresponds to C=C stretching of PVA. The band at approximately 1124 cm^{-1} corresponds to C—O stretching, and that at about 1780 cm^{-1} to C=O stretching of an unhydrolyzed ester functional group present on the PVA backbone.[19]

For the PVA/CS polymer blend, it was observed that the absorption peaks at about 3358 cm^{-1} and 3348 cm^{-1} associated with —OH stretching for neat PVA and CS, respectively, shifted to a lower wavenumber (3303 cm^{-1}). In addition, the peak observed at 1478 cm^{-1} that corresponded to —OH bending vibration of hydroxyl group in neat PVA shifted to a lower

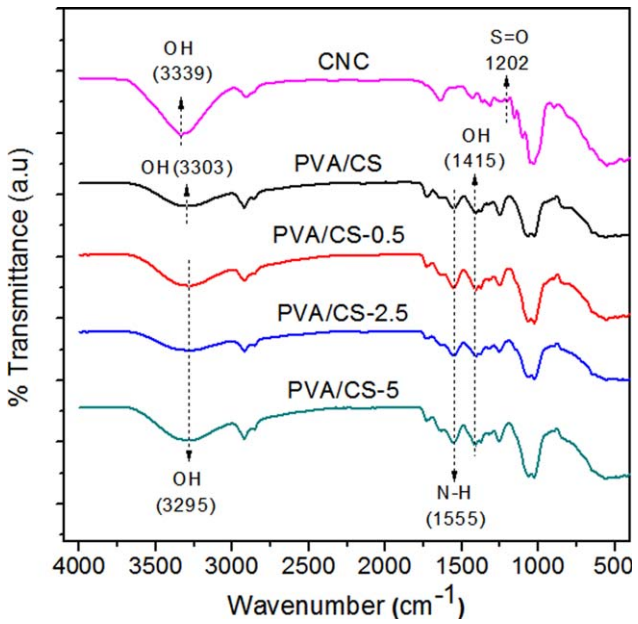

Figure 7. FTIR spectra of CNC and PVA/CS, PVA/CS-0.5, PVA/CS-2.5, and PVA/CS-5 bio-nanocomposite films. [Color figure can be viewed in the online issue, which is available at wileyonlinelibrary.com.]

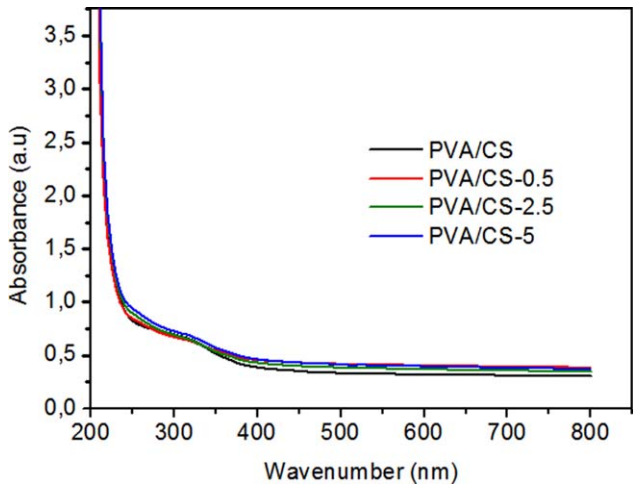

Figure 8. UV–Vis spectra of PVA/CS, PVA/CS-0.5, PVA/CS-2.5, and PVA/CS-5 bio-nanocomposite films. [Color figure can be viewed in the online issue, which is available at wileyonlinelibrary.com.]

frequency (1415 cm^{-1}) in PVA/CS blend (Figure 7). These results suggested the formation of a hydrogen bond between the hydroxyl groups of CS and PVA.[12,19,21] For PVA/CS–CNC bio-nanocomposite films, the peak observed at 3339 cm^{-1} associated to —OH stretching vibrations in the CNC spectrum, shifted to 3295 cm^{-1} in the PVA/CS–CNC bio-nanocomposites (Figure 7). Additionally, the band observed at 1592 cm^{-1} (N—H) in neat CS spectrum is shifted to 1555 cm^{-1} in PVA/CS–CNC spectra, confirming that strong interactions occurred between NH_3^+ group of CS and SO_3^- group (1202 cm^{-1}) of CNC. These observations indicated that strong electrostatic interactions and hydrogen bonding occurred between the functional groups of CNC and the free functional groups of PVA/CS polymer blend, as proposed in Figure 5(c). These results were also observed in cellulose fibers filled starch/PVA composite films.[18]

UV–Vis Absorbance of Films

The structure, optical absorption, and local dispersion of CNC for PVA/CS film and PVA/CS–CNC bio-nanocomposite films were studied by UV–vis absorption. The UV–Vis spectra of such films are presented in Figure 8. Evidently, the PVA and CS films are transparent in the UV–Vis region, resulting in a very low absorption level, as shown in Supporting Information Figure S5. After blending, the PVA/CS polymer blend showed the same behavior of that observed for neat polymers (Figure 8), indicating that these polymers were well blended because of their high compatibility.[19] Furthermore, when CNC were added to the PVA/CS polymer blend, all the investigated PVA/CS–CNC bio-nanocomposite films maintained the same absorption level of the PVA/CS polymer blend. This observation confirmed that the clarity of PVA/CS was not affected by the addition of CNC, as visually observed for the as-prepared films [Figure 5(b)]. Because the CNC are smaller than the wavelength of visual light (shown by AFM analysis), the UV–Vis results of bio-nanocomposite films confirmed that the CNC were dispersed/distributed in nanoscale within the PVA/CS matrix. This is directly related to strong interfacial interactions between the macromolecular chains of polymers and the surface of CNC, as evidenced by FTIR measurements (Figure 7).

SEM Characterization of Films

The SEM photographs of the cryo-fractured sections of PVA/CS and PVA/CS–CNC films are shown in Supporting Information Figure S6. It was observed that the cross-section of unloaded PVA/CS film was smooth without any cracks and pores [Supporting Information Figure S6(a)]. The cross-section of the PVA/CS–CNC bio-nanocomposite film was relatively rougher than the PVA/CS film [Supporting Information Figure S6(b–d)]. One can clearly see that no obvious aggregations of CNC and microphase separation were observed from the SEM photographs. This indicates that CNC were dispersed homogenously within the PVA/CS blend, resulting in a high contact area with polymeric chains, and thus formed a stronger interaction and adhesion on the interfaces of CNC and macromolecular chains of PVA/CS. The excellent dispersion of CNC in the blend matrix was directly correlated with its effectiveness in improving the properties of bio-nanocomposite films.

Thermal Properties of Films

Thermogravimetric analysis (TGA) is considered the most important method for studying the thermal stability of polymers and polymer nanocomposites. Herein, the thermal stability of PVA/CS and PVA/CS–CNC films was studied in air atmosphere. The obtained TGA and DTG curves are presented in Figure 9(a,b), respectively. For all investigated films, the first weight loss observed that occurred at about 100°C was related to evaporation of absorbed water. It should be noted that the amount of absorbed water for unloaded PVA/CS film is higher than that of PVA/CS–CNC bio-nanocomposite films, suggesting that the CNC were well dispersed within the PVA/CS matrix, acting as an interpenetrated network within the polymer blend matrix, thus preventing the absorption of water by films when exposed to the moisture. From a practical point of view, it is clear that the thermal stability of PVA/CS–CNC bio-nanocomposite films increased with the addition of CNC. To evaluate the effect of addition of CNC on the onset temperature of degradation of the films, analysis of the TGA data was done on the basis of the temperature corresponding to a weight loss of 15% ($T_{15\%}$). For PVA/CS polymer blend, the $T_{15\%}$ was determined at 194°C which associated to the degradation of the molecules of polymers. When CNC was added, the $T_{15\%}$ for PVA/CS-0.5, PVA/CS-2.5, and PVA/CS-5 bio-nanocomposite films was determined at 240, 241, and 253°C, respectively. These results indicated that the thermal stability of bio-nanocomposites was largely improved with addition of CNC. More importantly, the $T_{15\%}$ value for PVA/CS-5 is significantly higher than that of PVA/CS-0.5 and PVA/CS-2.5 samples. This could be due to the formation of more compact network that generated from the addition of relatively high content of CNC within the PVA/CS blend. As mentioned above, the CNC are thermally instable nanomaterials, the degradation process starts at 150°C (Figure 4), because the presence of sulfate groups on their surface. After their incorporation into polymer matrix, a complex network can be formed in bio-nanocomposite films via strong noncovalent interactions between the surface functionality of CNC and the macromolecular chains of polymers. Indeed,

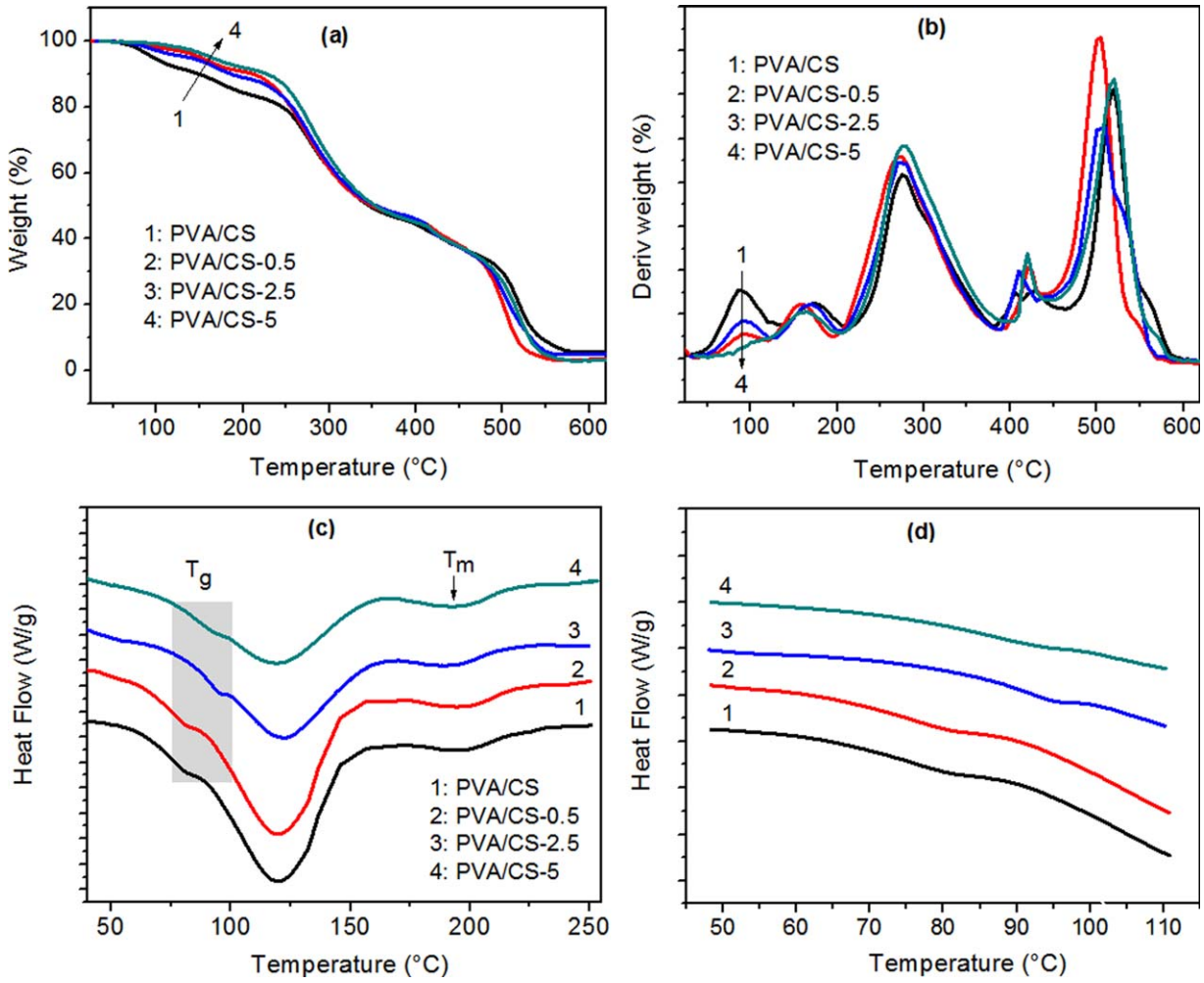

Figure 9. (a) TGA, (b) DTG, and (c) DSC curves of PVA/CS, PVA/CS-0.5, PVA/CS-2.5, and PVA/CS-5 bio-nanocomposite films and (d) T_g of the films. [Color figure can be viewed in the online issue, which is available at wileyonlinelibrary.com.]

in the bio-nanocomposite films, the major mass loss (≈50%) of CNC occurring between 150 and 300°C disappeared, suggesting a good interaction between the functional groups of CNC and the macromolecular chains of PVA/CS polymer blend. This leads in a mobility suppression of the polymer segments at the interfaces between PVA/CS and CNC surface, improvement in turn the thermal stability of PVA/CS blend.

The thermal transitions and melting behavior of PVA/CS blend and PVA/CS–CNC films were studied using differential scanning calorimetry (DSC), and the obtained curves are presented in Figure 9(c,d).

It should be noted that the glass temperature (T_g) of neat CS has been the subject of controversy, and variables such as the source or the extraction method strongly influence the T_g of CS.[56] Sakurai *et al.*[57] observed the T_g of CS at 203°C, while Kittur *et al.*[58] did not find evidence of a T_g, suggesting that the T_g for CS could lie at a higher temperature where degradation prevents its determination. According to Tripathi *et al.*,[59] DSC thermogram of CS exhibited a sharp exothermic peak at 290°C, associated with the decomposition of CS. In our work, neat CS did not show any significant transition in the temperature range of the DSC scans.[19,60]

The DSC curves of PVA/CS showed three thermal transitions, the first at about 74°C, indicating the glass transition (T_g) of PVA. The second transition occurred at about 100–120°C, indicating the loss of absorbed water. The third transition occurred at about 193°C, indicating the melting of PVA polymer.[58] The PVA/CS–CNC bio-nanocomposite films showed the same behavior of that observed for the PVA/CS blend, where three thermal transitions were observed [Figure 9(c)]. However, the T_g of PVA in the bio-nanocomposite films increased from 74°C for the PVA/CS blend to 88°C for the PVA/CS-5 bio-nanocomposite film [Figure 9(d)]. This can be explained by the strong interfacial interactions between the continuous phase and the dispersed phase. The T_m of PVA in the PVA/CS–CNC bio-nanocomposite films was not largely affected by the addition of CNC compared to the PVA/CS blend.

Tensile Properties of Films

The tensile properties of the neat PVA, neat CS, PVA/CS blend, and PVA/CS–CNC films were investigated by uni-axial tensile

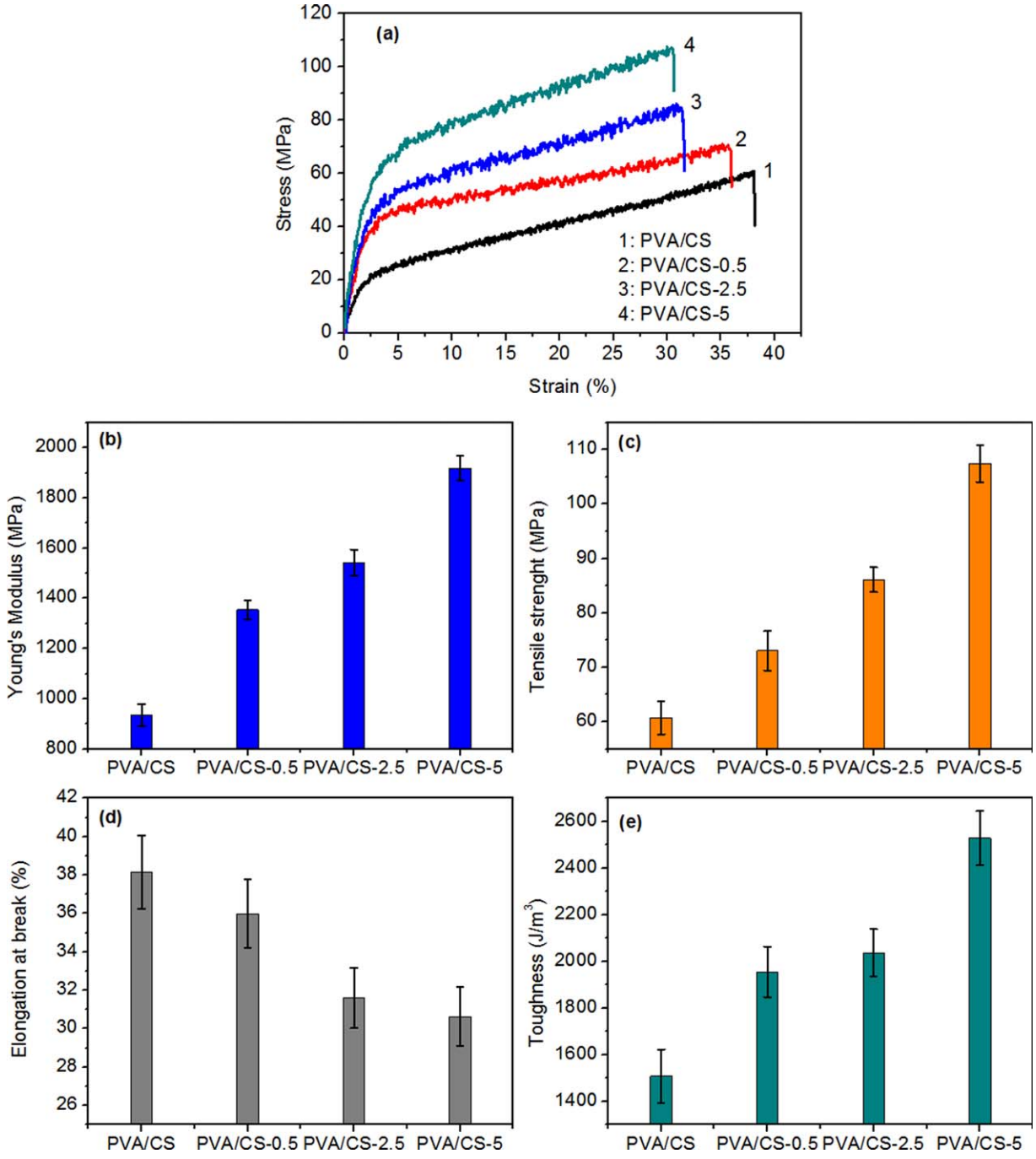

Figure 10. (a) Typical stress–strain curves of PVA/CS, PVA/CS-0.5, PVA/CS-2.5, and PVA/CS-5 bio-nanocomposite films, and plot of (b) Young's modulus, (c) tensile strength, (d) elongation at break, and (e) toughness as function of CNC content. [Color figure can be viewed in the online issue, which is available at wileyonlinelibrary.com.]

tests. Figure 10(a) shows the typical stress–strain curves for PVA/CS and PVA/CS–CNC films (the curves of neat PVA and neat CS are presented in Supporting Information Figure S7). From the stress–strain curves, the elongation at break (ε_b), the ultimate tensile strength (σ_s), the Young's modulus (E), and the toughness (T) of PVA/CS and PVA/CS–CNC films are extracted and presented as functions of CNC contents in Figure 10(b–e), and the values of these selected properties are presented in Supporting Information Table S1. The Young's modulus [Figure 10(b)] can be defined as the slope of the linear elastic deformation of the stress–strain curve, the ultimate tensile strength [Figure 10(c)] represents the maximum stress value applied to the material, the elongation at break [Figure 10(d)] is defined as the strain to break of the material, and the toughness [Figure 10(e)] is the energy needed to break the material, and can be calculated from the area under the stress–strain curve.

According to the results of stress–strain curves illustrated in Figure 10(a) and Supporting Information Figure S7, the tensile properties of neat PVA and neat CS are affected by their blending and the addition of the different amounts of CNC. The neat PVA film exhibits an elongation at break of 64.98%, an ultimate tensile strength of 49.80 MPa, a Young's modulus of 865.78 MPa, and a toughness of 2344.57 $\times$ 10^6 J m^{-3} (Supporting Information Table S1). Notably, due to the high molecular weight of CS, its solvent casted film is a mechanically brittle material. The CS film has an elongation at break of 14.49%, ultimate tensile stress of 51.48 MPa, Young's modulus of 1219.76 MPa, and toughness of 618.66 $\times$ 10^6 J m^{-3} (Supporting Information Table S1). These selected tensile properties of the neat PVA and neat CS films were affected after blending in PVA/CS film. Thus, the elasto-plastic behavior of the PVA/CS film is the same to that of neat PVA and neat CS films, with little variation of the indicated tensile properties. The PVA/CS film exhibits an elongation at break of 38.14%, an ultimate tensile strength of 60.73 MPa, a Young's modulus of 933.69 MPa, and a toughness of 1507.37 $\times$ 10^6 J m^{-3}. These new values observed for PVA/CS film in comparison with neat PVA and CS suggest the establishment of bonds between the chains of both PVA and CS polymers in the blend, as deduced from the FTIR spectra (Figure 6). These bonds reinforce the network structure, thus modifying the tensile properties of the PVA/CS film.[19] These results are comparable to those reported by other authors working with PVA/CS polymer blends.[19,20]

For PVA/CS–CNC bio-nanocomposite films, after the addition of CNC into the PVA/CS blend, a remarkable increase of tensile properties was clearly visible, especially in: (i) the ultimate tensile strength, (ii) the modulus, and (iii) the toughness [Figure 10(e)]. This could be due to the formation of a more bonded network that was generated by the addition of CNC within the PVA/CS blend. This network was formed throughout the strong electrostatic interactions and hydrogen bonding that occurred between the CNC and PVA/CS polymer blend.

In regard to PVA/CS blend, the Young's modulus and tensile strength of the PVA/CS–CNC bio-nanocomposite increased by 105%, from 933.69 to 1917.62 MPa [Figure 10(b)], and by 77%, from 60.73 to 107.45 MPa [Figure 10(c)] when 5 wt % CNC was added. Such improvements confirm that PVA/CS–CNC bio-nanocomposite films are mechanically strong materials. Furthermore, it should be noted that in comparison to the uncharged PVA/CS blend, the PVA/CS–CNC films not only have a higher strength and modulus but also a higher toughness that reaches a maximum value of 2529.03 $\times$ 10^6 J m^{-3} for the PVA/CS-5 bio-nanocomposite film.

The elongation at break of PVA/CS was not largely affected by the addition of CNC; a decrease from 38% for unloaded PVA/CS to 30% for PVA/CS-5 occurred [Figure 10(e)]. The gradual increase of the toughness and the slight decrease of the elongation at break determined for the PVA/CS–CNC bio-nanocomposite films confirm that these films are mechanically flexible materials.

Apparently, the large surface area and very high Young's modulus of CNC are responsible for the significant reinforcement impact on mechanical properties of the PVA/CS blend. In addition, homogeneous dispersion of CNC along with favorable interfacial interactions between CNC and the polymeric matrix is essential to achieve improvement in the final tensile properties of the as-prepared bio-nanocomposite films. These ideal conditions result in mechanically strong and flexible bio-plastic films.

CONCLUSION

High-performance novel polymer bio-nanocomposite films were prepared via a solution casting of polyvinyl alcohol (PVA), chitosan (CS), and cellulose nanocrystals (CNC). The CNC used as nanoreinforcing agents were isolated at the nanometric scale from sugarcane bagasse, via sulfuric acid hydrolysis process; then they were characterized and successfully dispersed into PVA/CS blend to produce PVA/CS–CNC bio-nanocomposite films. The structural characterizations showed that the PVA and CS were perfectly compatible and miscible polymers via the hydrogen bond interactions between the hydroxyl groups of PVA and CS, thus resulting in the formation of a new biocompatible homogeneous blend matrix for bio-nanocomposite development. As evidenced by the viscosity measurement of film-forming solutions and microscopic and spectroscopic observations of bio-nanocomposite films, it was found that the CNC formed an interconnected bond network throughout strong electrostatic interactions and hydrogen bonding between hydroxyl groups and anionic sulfate groups of CNC and the hydroxyl and amine groups of the PVA/CS polymeric blend. These strong bonds ensure the high compatibility between the CNC and the bio-nanocomposite films, thus confirming that the CNC were well dispersed within the PVA/CS. As a result, the thermal stability, glass transition temperature, and tensile properties of bio-nanocomposite films gradually increased with the increase of CNC contents. By adding 5 wt % CNC, there was a 30% increase of thermal stability, 19% increase of glass transition temperature, 105% increase of Young's modulus, 77% increase of tensile strength, and 68% increase of toughness achieved. This work was performed to valorize the Moroccan sugarcane bagasse for the production of nanosized cellulose crystals, and to study its ability to reinforce bio-polymer blends to produce the aforementioned bio-nanocomposite films with good thermal and mechanical properties.

ACKNOWLEDGMENTS

The financial assistance of the OCP Group (Office Chérifien des Phosphates in the Moroccan Kingdom) towards this research is hereby acknowledged. The authors are also grateful to COSUMAR Company in Morocco for providing us the raw sugarcane bagasse. We equally thank all administrative and technical support teams of the UM6P, particularly Pr. Nicolas Cheimanoff (Dean of EMINES - School of Industrial Management).

REFERENCES

1. Rodríguez-González, C.; Martínez-Hernández, A. L.; Castaño, V. M.; Kharissova, O. V.; Ruoff, R. S.; Velasco-Santos, C. *Ind. Eng. Chem. Res.* **2012**, *51*, 3619.

2. Goffin, A. L.; Raquez, J. M.; Duquesne, E.; Siqueira, G.; Habibi, Y.; Dufresne, A.; Dubois, P. *Biomacromolecules* **2011**, *12*, 2456.
3. Kanmani, P.; Rhim, J.-W. *Carbohydr. Polym.* **2014**, *106*, 190.
4. Rogovina, S. Z.; Alexanyan, C. V.; Prut, E. V. J. *J. Appl. Polym. Sci.* **2011**, *121*, 1850.
5. Vasconcellos, F. C.; Goulart, G. A. S.; Beppu, M. M. *Powder Technol.* **2011**, *205*, 65.
6. El Achaby, M.; Essamlali, Y.; El Miri, N.; Snick, A.; Abdelouahdi, K.; Fihri, A.; Zahouily, M.; Solhy, A. *J. Appl. Polym. Sci.* **2014**, 131.
7. Jayakumar, R.; Prabaharan, M.; Nair, S. V.; Tokura, S.; Tamura, H.; Selvamurugan, N. *Prog. Mater. Sci.* **2010**, *55*, 675.
8. Dash, M.; Chiellini, F.; Ottenbrite, R. M.; Chiellini, E. *Prog. Polym. Sci.* **2011**, *36*, 981.
9. Butler, B. L.; Vergano, P. J.; Testin, R. F.; Bunn, J. M.; Wiles, J. L. *J. Food Sci.* **1996**, *61*, 953.
10. Park, S. Y.; Marsh, K. S.; Rhim, J. W. *J. Food Sci.* **2002**, *67*, 194.
11. Sionkowska, A. *Prog. Polym. Sci.* **2011**, *36*, 1254.
12. Costa-Júnior, E. S.; Barbosa-Stancioli, E. F.; Mansur, A. A. P.; Vasconcelos, W. L.; Mansur, H. S. *Carbohydr. Polym.* **2009**, *76*, 472.
13. Dias, L.; Mansur, L. S.; Donnici, H. S.; Pereira, C. L. *Biomatter* **2011**, *1*, 114.
14. Wang, J.; Wang, X.; Xu, C.; Zhang, M.; Shang, X. *Polym. Int.* **2011**, *60*, 816.
15. Santos, C.; Silva, C. J.; Büttel, Z.; Guimarães, R.; Pereira, S. B.; Tamagnini, P.; Zille, A. *Carbohydr. Polym.* **2014**, *99*, 584.
16. Pandele, A. M.; Ionita, M.; Crica, L.; Dinescu, S.; Costache, M.; Iovu, H. *Carbohydr. Polym.* **2014**, *102*, 813.
17. Chhatri, A.; Bajpai, J.; Bajpai, A. K.; Sandhub, S. S.; Jain, N.; Biswas, J. *Carbohydr. Polym.* **2011**, *83*, 876.
18. El-Sayed, S.; Mahmoud, K. H.; Fatah, A. A.; Hassen, A. *Phys. B: Condens. Matter* **2011**, *406*, 4068.
19. Bonilla, J.; Fortunati, E.; Atarés, L.; Chiralt, A.; Kenny, J. M. *Food Hydrocolloid* **2014**, *35*, 463.
20. Bahrami, S. B.; Kordestani, S. S.; Mirzadeh, H.; Mansoori, P. *Iran. Polym. J.* **2003**, *12*, 139.
21. Jia, Y. T.; Gong, J.; Gu, X. H.; Kim, H. Y.; Dong, J.; Shen, X. Y. *Carbohydr. Polym.* **2007**, *67*, 403.
22. Chivrac, F.; Pollet, E.; Avérous, L. *Mater. Sci. Eng.* **2009**, *67*, 1.
23. Paul, D. R.; Robeson, L. M. *Polymer* **2008**, *49*, 3178.
24. Alexandra, M.; Dubois, P. *Mater. Sci. Eng.* **2000**, *28*, 1.
25. Petersson, L.; Oksman, K. *Compos. Sci. Technol.* **2006**, *66*, 2187.
26. Habibi, Y.; Lucia, L. A.; Rojas, O. *J. Chem. Rev.* **2010**, *110*, 3479.
27. Fortunati, E.; Puglia, D.; Luzia, F.; Santullic, C.; Kenny, J. M.; Torre, L. *Carbohydr. Polym.* **2013**, *97*, 825.
28. Mariano, M.; El Kissi, N.; Dufresne, A. *J. Polym. Sci., Part B: Polym. Phys.* **2014**, *52*, 791.
29. Azizi-Samir, M. A. S.; Alloin, F.; Sanchez, J. Y.; Dufresne, A. *Polymer* **2004**, *45*, 4149.
30. Sturcová, A.; Davies, G. R.; Eichhorn, S. J. *Biomacromolecules* **2005**, *6*, 1055.
31. Brinchi, L.; Cotana, F.; Fortunati, E.; Kenny, J. M. *Carbohydr. Polym.* **2013**, *94*, 154.
32. Li, J.; Wei, X.; Wang, Q.; Chen, J.; Chang, G.; Kong, L.; Su, J.; Liu, Y. *Carbohydr. Polym.* **2012**, *90*, 1609.
33. Teixeira, E. D. M.; Bondancia, T. J.; Teodoro, K. B. R.; Corrêa, A. C.; Marconcini, J. M.; Mattoso, L. H. C. *Ind. Crop. Prod.* **2011**, *33*, 63.
34. Mandal, A.; Chakrabarty, D. *Carbohydr. Polym.* **2011**, *86*, 1291.
35. Bras, J.; Hassan, M. L.; Bruzesse, C.; Hassan, E. A.; ElWakil, N. A.; Dufresne, A. *Ind. Crop. Prod.* **2010**, *32*, 627.
36. Martínez, E. A.; Silva, S. S.; Silva, J. B. A.; Solenzal, A. I. N.; Felipe, M. G. A. *Process Biochem.* **2003**, *38*, 1677.
37. Hernández-Salas, J. M.; Villa-Ramírez, M. S.; Veloz-Rendón, J. S.; Rivera-Hernández, K. N.; González-César, R. A.; Plascencia-Espinosa, M. A. *Bioresour. Technol.* **2009**, *100*, 1238.
38. Chandel, A. K.; Kapoor, R. K.; Singh, A.; Kuhad, R. C. *Bioresour. Technol.* **2007**, *98*, 1947.
39. Restuti, D.; Michaelowa, A. *Energy Policy* **2007**, *35*, 3952.
40. Quintero, J. A.; Montoya, M. I.; Sánchez, O. J.; Giraldo, O. H.; Cardona, C. A. *Energy* **2008**, *33*, 385.
41. Dos Santos, R. M.; Neto, W. P. F.; Silvério, H. A.; Martins, D. F.; Dantas, N. O.; Pasquini, D. *Ind. Crop. Prod.* **2013**, *50*, 707.
42. Jiang, F.; Esker, A. R.; Roman, M. *Langmuir* **2010**, *26*, 17919.
43. Espinosa, S. C.; Kuhnt, T.; Foster, E. J.; Weder, C. *Biomacromolecules* **2013**, *14*, 1223.
44. Mirhosseini, H.; Tan, C. P.; Hamid, N. S. A.; Yusof, S. *Colloids Surf. A* **2008**, *315*, 47.
45. Morais, J. P. S.; Rosa, M. D. F.; Filho, M. D. M. D. S.; Nascimento, L. D.; Nascimento, D. M. D.; Cassales, A. R. *Carbohydr. Polym.* **2013**, *91*, 229.
46. Flauzino-Neto, W. P. F.; Silvério, H. A.; Dantas, N. O.; Pasquini, D. *Ind. Crop. Prod.* **2013**, *42*, 480.
47. Eichhorn, S. J.; Dufresne, A.; Aranguren, M.; Marcovich, N. E.; Capadona, J. R.; Rowan, S. J.; Weder, C.; Thielemans, W.; Roman, M.; Renneckar, S.; Gindl, W.; Veigel, S.; Keckes, J.; Yano, H.; Abe, K.; Nogi, M.; Nakagaito, A. N.; Mangalam, A.; Simonsen, J.; Benight, A. S.; Bismarck, A.; Berglund, L. A.; Peijs, T. *J. Mater. Sci.* **2010**, *45*, 1.
48. Elazzouzi-Hafraoui, S.; Nishiyama, Y.; Heux, L.; Dubreuil, F.; Rochas, C. *Biomacromolecules* **2008**, *9*, 57.
49. Araki, J.; Wada, M.; Kuga, S.; Okano, T. *Colloids Surf. A* **1998**, *142*, 75.
50. Azubuike, C. P.; Rodriguez, H.; Okhamafe, A. O.; Rogers, R. D. *Cellulose* **2012**, *19*, 425.
51. Kumar, R.; Mago, G.; Balan, V.; Wyman, C. E. *Bioresour. Technol.* **2009**, *100*, 3948.
52. Peresin, M. S.; Habibi, Y.; Zoppe, J. O.; Pawlak, J. J.; Rojas, O. J. *Biomacromolecules* **2010**, *11*, 674.
53. Khan, A.; Khan, R. A.; Salmieri, S.; Le Tien, C.; Riedl, B.; Bouchard, J.; Chauve, G.; Tan, V.; Kamal, M. R.; Lacroix, M. *Carbohydr. Polym.* **2012**, *90*, 1601.

54. De Mesquita, J. P.; Donnici, C. L.; Pereira, F. V. *Biomacromolecules* **2010**, *11*, 473.

55. Singh, V.; Sharma, A. K.; Tripathi, D. N.; Sanghi, R. J. *J. Hazard. Mater.* **2009**, *161*, 955.

56. Neto, C. G. T.; Giacometti, J. A.; Job, A. E.; Ferreira, F. C.; Fonseca, J. L. C.; Pereira, M. R. *Carbohydr. Polym.* **2005**, *62*, 97.

57. Sakurai, K.; Maegawa, T. T.; Takahashi, T. *Polymer* **2000**, *41*, 7051.

58. Kittur, F. S.; Prashanth, K. V. H.; Udaya Sankar, K.; Tharanathan, R. N. *Carbohydr. Polym.* **2002**, *49*, 185.

59. Tripathi, S.; Mehrotra, G. K.; Dutta, P. K. *Int. J. Biol. Macromol.* **2009**, *45*, 372.

60. Nguyen, N. T.; Liu, J. H. *Eur. Polym. J.* **2013**, *49*, 4201.